Use of a C-Arm System to Generate True Three-dimensional Computed Rotational Angiograms: Preliminary In Vitro and In Vivo Results

R. Fahrig, A. J. Fox, S. Lownie, and D. W. Holdsworth

PURPOSE: To evaluate the potential use of a C-arm mounted X-ray image intensifier (XRII) system to generate three-dimensional computed rotational angiograms during interventional neuroradiologic procedures. **METHODS:** A clinical angiographic system was modified to allow collection of sufficient views during selective intraarterial contrast injections for CT reconstruction of a 15 × 15 × 15-cm^3 volume. Image intensifier distortion and C-arm instabilities were corrected by using image-based techniques. The impact of the pulsatile nature of the vessels during image data acquisition and of the presence of bone on the 3-D reconstructions was investigated by generating 3-D reconstructions of an anesthetized 20-kg pig and of a human skull phantom. **RESULTS:** A sequence of images sufficient for 3-D reconstruction was acquired in less than 5 seconds. Image intensifier distortion and C-arm instabilities were corrected to subpixel accuracy (0.035 mm and 0.07 mm, respectively). Both the intracranial vessels of the pig and the small, high-contrast structures in the skull were reconstructed with negligible artifacts. **CONCLUSIONS:** Using a C-arm mounted XRII system, computed rotational angiography can provide true 3-D images of diagnostic quality.

Index terms: Angiography, technique; Animal studies; Computed tomography, three-dimensional

AJNR Am J Neuroradiol 18:1507–1514, September 1997

An imaging system with three-dimensional capabilities suitable for use during interventional procedures must exhibit the following characteristics: it must have near-real-time fluoroscopic capabilities and roadmapping; it must provide accurate, quantitative 3-D anatomic information about the vessel lumen and the location of the embolization material; and it must allow unobstructed access to the patient during the intervention.

Several recent studies have shown the effectiveness of spiral computed tomographic (CT) angiography in the diagnosis of aneurysms and in the planning of treatment (1, 2). However, this technique has no capability for fluoroscopic imaging. Magnetic resonance angiography has also been used to evaluate intracranial aneurysms (3); however, signal loss due to slow flow and disturbed flow is well documented (4), and real-time imaging capabilities are still in the developmental stage (5). An additional technique that provides limited 3-D information about the cerebral vessels is rotational angiography (6). Digital images are acquired as a C-arm rotates through 30° to 180° during a selective arterial contrast injection. While the additional information is not quantitative, when the images are viewed in a cine loop the kinematic 3-D effect may resolve ambiguities about vessel configurations. We have developed and tested the necessary modifications to a clinical C-arm mounted X-ray image intensifier system that allow the generation of 3-D images during the endovascular procedure. We call this imaging technique *computed rotational angiography*. Although the raw projection data are sim-

Received October 1, 1996; accepted after revision March 7, 1997.

Supported in part by Siemens Medical Systems, by the Medical Research Council of Canada, and by the Heart and Stroke Foundation of Canada.

Presented at the annual meeting of the American Society of Neuroradiology, Seattle, Wash, June 1996.

From the Departments of Medical Biophysics (R.F., D.W.H.), Diagnostic Radiology (A.J.F., S.L., D.W.H.), and Clinical Neurological Sciences (A.J.F., S.L.), University of Western Ontario, and the J. P. Robarts Research Institute (R.F., A.J.F., D.W.H.), London, Ontario, Canada.

Address reprint requests to Rebecca Fahrig, the J. P. Robarts Research Institute, 100 Perth Dr, PO Box 5015, London, Ontario N6A 5K8, Canada.

AJNR 18:1507–1514, Sep 1997 0195-6108/97/1808–1507

Comparison of the two imaging systems used for data acquisition

	Conventional System	High-Speed System
XRII maximum nominal diameter, cm	27	40
Maximum possible rotation, degrees	270	305
Speed of rotation, degrees per second	15	45
Rate of image acquisition, frames per second	7.5	30
Total time for image acquisition, s	13.3	4.4
Focal spot-to-detector distance, cm	87	120
Geometric magnification at the isocenter	1.2	1.5
No. of images acquired per 3-D reconstruction	100	130

Note.—XRII indicates X-ray image intensifier.

ilar to the images produced by rotational angiography, reconstruction of these projection data with CT results in a 3-D image with isotropic resolution. The computed volume image provides quantitative measurements with higher spatial resolution than does helical CT angiography. We describe the steps taken to implement the modifications and illustrate the quality of images that we achieved.

Materials and Methods

Image Acquisition

Image data were acquired using a conventional clinical biplane angiographic system (only one plane used during image acquisition) and a modified high-speed single-plane system. The characteristics of both systems are summarized in the Table.

Images were acquired while the C-arm rotated around the object of interest, resulting in approximately 130 images over the 200° required for the volume reconstruction. Exposure time was usually less than 20 milliseconds per frame. The tube voltage ranged from 73 to 110 kVp, and the tube current ranged from 100 to 500 mA.

During the rotation of the C-arm, a selective injection of contrast agent was administered through a catheter. We have not yet optimized the injection protocol for this imaging technique, although a previous in vivo study showed that an injection rate of 4 mL/s, with a 1-second delay before imaging, achieved satisfactory vascular detail with minimal postprocessing (6).

After correcting the projection images as described below, the volume images were reconstructed by using a standard fan-beam algorithm (convolution back-projection [7]) currently used in CT scanners, or by using a Feldkamp cone-beam reconstruction method (8). The convolution back-projection method is sufficient for reconstruction of a limited region close to the central section of the volume, and may lead to faster reconstruction times if implemented with dedicated hardware. However, for larger volumes, the Feldkamp method produces improved results in sections far away from the central one, and is therefore preferred when reconstruction time is not a constraint. Our reconstruction protocol did not implement the fan-beam technique with dedicated hardware, and our code was not optimized for speed of reconstruction; however, volumes could be obtained within approximately 1 hour. We estimate that the same volumes could now be generated in under 10 minutes by using a single desk-top workstation with a hardware accelerator.

The 3-D reconstructions had isotropic pixels, approximately 0.5 mm on a side, and covered a volume of approximately $13 \times 13 \times 13$ cm^3. The volume images were viewed using several display modes, including maximum intensity projection (MIP), multiplanar reformatting for viewing sections through the volumes at arbitrary angles, surface or volume rendering of the vessels, and radiographic reprojection. Display threshold (window and level) could be selected interactively (after reconstruction) to provide optimum visibility of vascular detail.

Total Image Acquisition Time

This issue was addressed by suitably modifying the drive motor on the C-arm of the prototype high-speed digital angiographic unit. The speed of rotation was increased to 45° per second, a threefold increase over the conventional system. The total acquisition time was 4.4 seconds during a rotation through 200°. The configuration of the digital imaging system allowed acquisition of images at up to 30 frames per second, ensuring that at least 130 images were acquired per rotation.

X-Ray Image Intensifier (XRII) Distortion Correction

Distortion in XRIIs can be separated into two categories: that caused by mapping of a flat image onto a curved input phosphor (pincushion distortion), and that caused by the deflection of electrons in the earth's magnetic field. The first effect is independent of the orientation of the XRII; however, the second effect depends on the path of the electrons through the earth's magnetic field and is therefore dependent on orientation. We characterized and corrected for both effects by fixing a rectilinear grid of small steel beads (1.66 mm in diameter, with a center-to-center spacing of 1 cm) to the front of the XRII. Correction was achieved by ensuring that the beads maintained their exact spacing and absolute location in every image. A different, angle-dependent correction must be applied to each image. This technique has been described in detail elsewhere (9).

C-Arm Stability

Several effects cause the motion of the C-arm to deviate from a perfect circular path during image acquisition. Sag

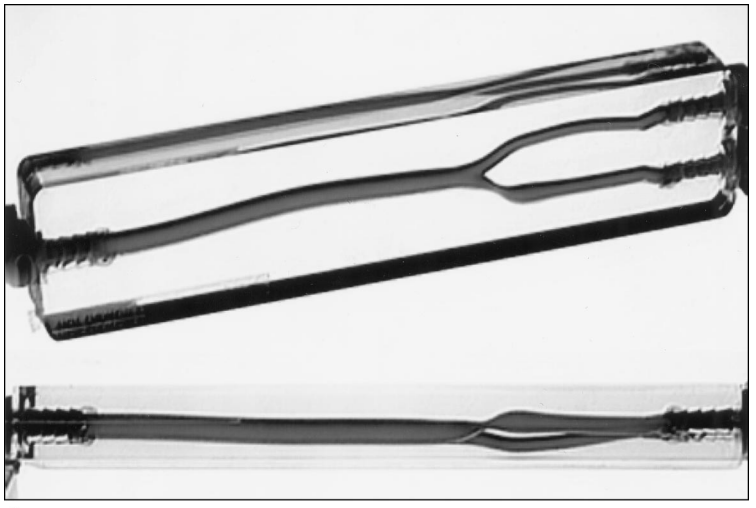

A

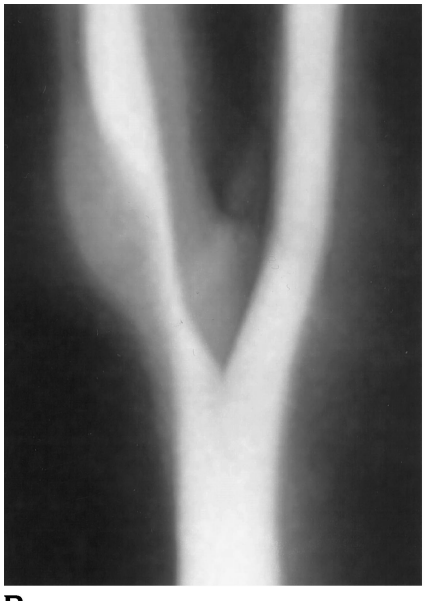

B

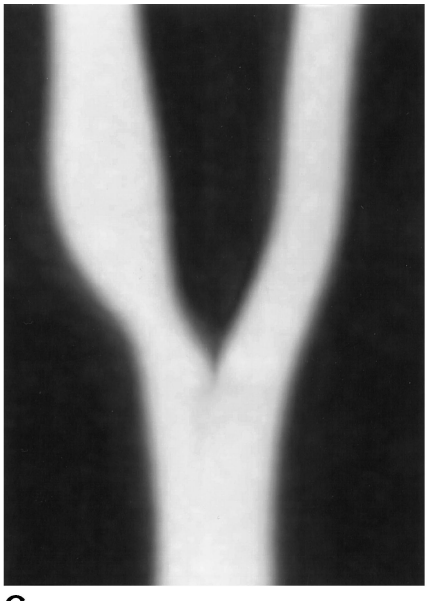

C

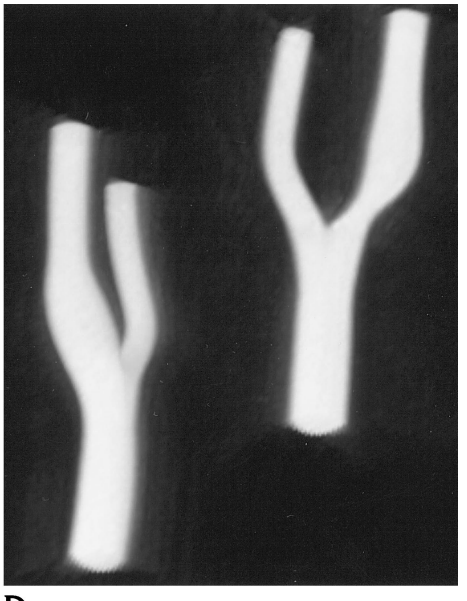

D

Fig 1. *A*, Photograph of the lucite model of the carotid bifurcation with a 30% stenosis (according to the NASCET index).

B, MIP image through a 3-D CT reconstruction of one half of the model of the carotid bifurcation. The 2-D projection data were not corrected for XRII distortion and gantry instability before reconstruction. Note significant blurring at the bifurcation and halo artifacts at the periphery of the vessels.

C, MIP image through a 3-D reconstruction of the same data after corrections were made for XRII distortion and gantry instabilities.

D, Double oblique MIP image through the full 3-D data set of the bilateral neck phantom shows normal (*left*) and 30% stenosed (*right*) vessels.

occurs as a result of the weight of the material suspended at the two ends of the C-arm, transient vibration occurs during the acceleration of the C-arm, and a spiraling motion may result from the gears that drive the rotation of the C-arm. All three effects must be corrected for before an accurate reconstruction can be achieved.

We characterized these motions by tracing the center of a high-contrast object (a large steel ball, 16.2 mm in diameter, which was fixed to the angiographic patient table) from frame to frame as the C-arm rotated. The correction approach we used was based on two assumptions: first, that the motion of the C-arm/imaging chain is reproducible during rotation and, second, that the deviations from a perfect circle are small. Under these conditions, motion of the C-arm may be corrected by applying subpixel shifts to the images as a function of angle of acquisition. The details of the correction have been described previously (9).

The impact of the corrections for XRII distortion and for C-arm stability was demonstrated by imaging a model of the carotid bifurcations of the neck. The model (Fig 1) consisted of a 16-cm-diameter cylinder filled with water, into which were placed two anthropomorphic phantoms of the carotid bifurcation (10, 11). The bifurcations were filled with 150 mg/mL iodinated contrast agent, and images were acquired using the conventional angiographic unit. It is important to test the correction processes in a model for which the geometry of the vessels is known exactly—one of the bifurcations represented a 30% stenosis (according to the North American Symptomatic Carotid Endarterectomy Trial [NASCET] index [12]) and the other was normal (−60% by the NASCET index).

Impact of In Vivo Motions on Reconstructions

We expected that the pulsatile nature of blood flow, the change in diameter of the blood vessels during the cardiac cycle, and motion caused by the respiratory cycle would have a significant effect on our ability to reconstruct 3-D volume data sets. To test this hypothesis, we obtained in vivo images of the intracranial vessels of a 20-kg anesthetized pig. These were preliminary images, obtained during a 4.4-second imaging sequence of the high-speed angiographic unit. Contrast agent (300 mg/mL) was injected into the left carotid artery at 3 mL/s over 6 seconds (total contrast of 18 mL). The 3-D volume was reconstructed using the Feldkamp technique after applying the above corrections for XRII distortion and C-arm instability.

Reconstruction in the Presence of Dense Material Such as Bone

The reconstruction technique we used is the standard algorithm used in CT scanners today. We therefore expected the presence of artifacts at the boundaries between materials of different densities to be significant. In addition, we thought our ability to detect small objects might be limited by the relatively small number of two-dimensional projections used to reconstruct the volumes. To test this hypothesis, we reconstructed an ex vivo human skull (The Phantom Laboratory, Salem, NY). The skull was placed in air, and 100 projection images were acquired using the conventional system. The 3-D volume was reconstructed using the stacked-fan beam convolution back-projection technique after applying the above corrections for XRII distortion and C-arm instability.

Results

Total Image Acquisition Time

To acquire a data set sufficient for reconstruction, we required the C-arm to rotate through 200° with a constant velocity. Measurement of the time course of the modified C-arm after the initiation of rotation indicated that acceleration to 45° per second occurs in under 0.5 seconds. The C-arm then rotates smoothly at 45° per second, with a standard deviation of approximately 1.5% in velocity (maximum deviation from the average of 7%) through the required 200°. Modifications to the system allowed rotation through 200° within 4.4 seconds.

XRII Distortion Correction

A previous investigation (9) has shown that it is possible to correct for image distortion such that the mean residual error is only 0.07 pixels. This represents a mean displacement, after correction, of only 0.04 mm. The maximum displacement, after correction, was found to be 0.26 pixels, or only 0.13 mm. The spatial distribution of the small amount of distortion that remains after correction does not demonstrate any particular pattern, which indicates that all regions of the XRII have been properly corrected for distortion and can be used to calculate 3-D volume reconstructions.

C-Arm Stability

Our technique for characterizing nonstandard motions of the C-arm indicates that, although some motions of the C-arm are significant, the C-arm motion is reproducible to within ±0.13 pixels, or 0.07 mm (9). We can therefore correct for all categories of nonstandard motions of the C-arm by applying a predetermined shift to each projection image before calculating the 3-D volume reconstructions.

The results of the reconstruction of the contrast-filled vessel phantom (Fig 1) illustrate our ability to correct for both XRII distortion and nonstandard motions of the C-arm. The zone of blurring in 3-D reconstructions using uncorrected data (Fig 1B) can be as large as 1 cm in extent in the axial direction owing to the spiraling motion of the C-arm as it rotates. In the lateral direction, image blur in the uncorrected data is caused mainly by the angle-dependent distortion in the XRII. To verify the geometric fidelity of the images generated from corrected data, we measured the percentage of stenosis on the MIP image and found it to be 33% (by diameter), which compares well with the true value of 30%. Filling with 50% contrast agent produced a signal of approximately 8800 Hounsfield units (HU) on a background noise of approximately 160 HU in the reconstruction.

Impact of In Vivo Motions on Reconstructions

The 3-D reconstruction of the intracranial vessels of an anesthetized pig (Fig 2) illustrates our ability to reconstruct vessels in the presence of pulsatile flow, cardiac pulsation, and respiratory motion. The measured signal in the left carotid vessel lumen was approximately 11 000 HU on a background noise of about 160 HU in the reconstruction. Of particular interest in this 3-D volume image is the clear reconstruction of the vessels intracranially on the right. In this case, the right common carotid artery and jugular vein were occluded, and delayed filling of the right side of the brain therefore occurred through the rete (Fig 2E). Filling was, however,

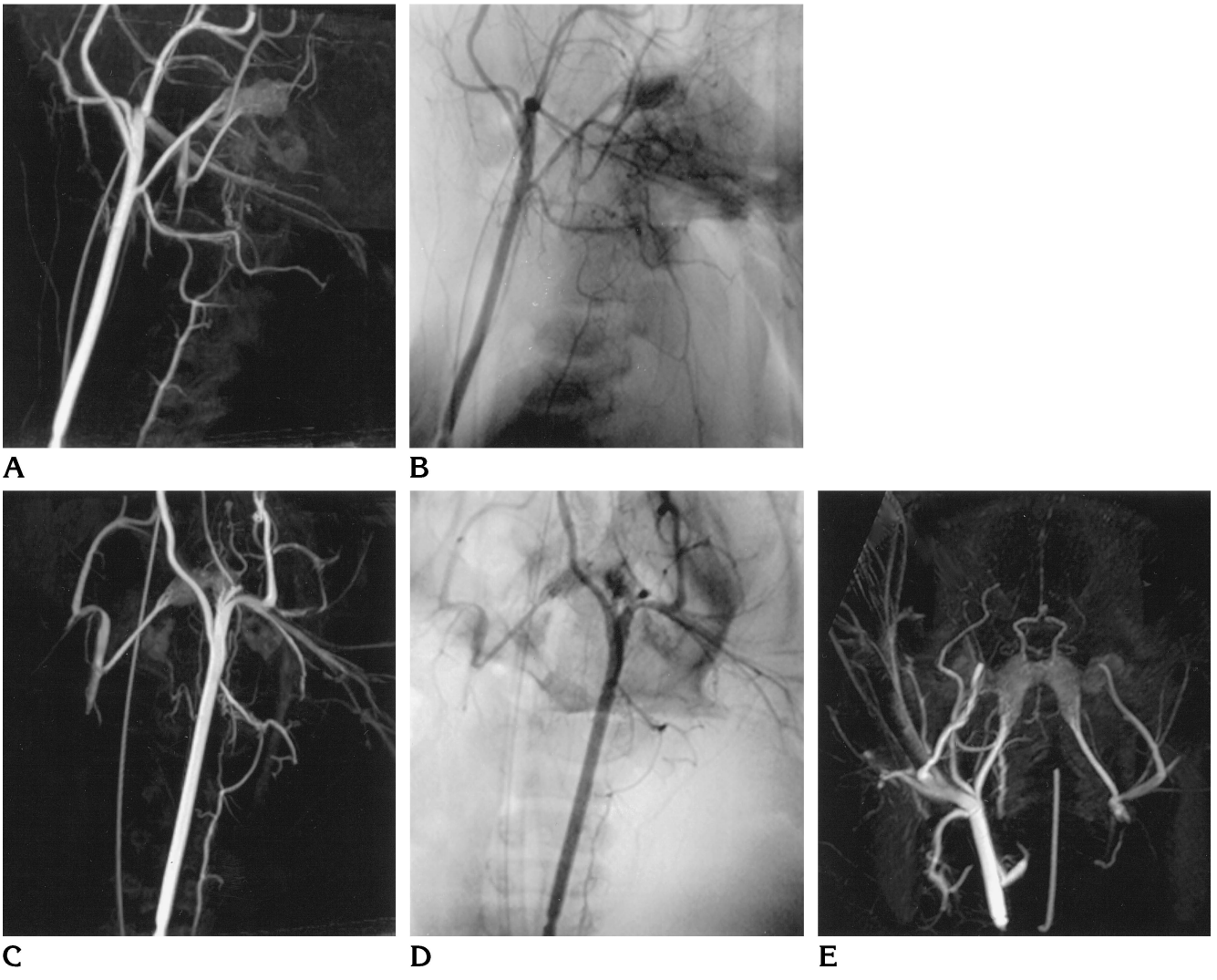

Fig 2. Comparison of a single 3-D volume reconstruction of an anesthetized pig with the original 2-D radiographic projections.

A and *C*, Lateral and anteroposterior views in MIP through the 3-D volume.

B and *D*, 2-D lateral and AP projection images, matched to *A* and *C*. Note the faithful reconstruction of small vessels in the MIP images as compared with the vessels that are visible in the 2-D projection images.

E, Craniocaudal MIP image through the 3-D volume. This view is not normally available to the interventionalist during patient treatment. The small, straight object (*center bottom*) to the right of the carotid indicates the presence of a high-contrast marker within the endotracheal tube.

delayed by approximately 0.5 seconds relative to the initiation of injection and image acquisition. This delay (and the resultant presence of inconsistencies in the acquired data set) does not seem to have a detrimental impact on the quality of the reconstruction as compared with the original projection images.

Image Reconstruction in the Presence of High-Density Tissue Such as Bone

A 3-D volume data set of the skull was produced (Fig 3). Artifacts within the bone were relatively low, and fine detail was easily visible in the sections, although some ripple in the surface of the bone was present in the surface-rendered images. This was probably due to the relatively low number of views (about 100) that were used to generate the reconstruction. The absence of other artifacts may be attributed to two factors: first, the system has isotropic resolution (ie, the same pixel spacing in all three directions) and, second, the pixels are small. Both characteristics reduce nonlinear partial volume effects and therefore lead to fewer artifacts.

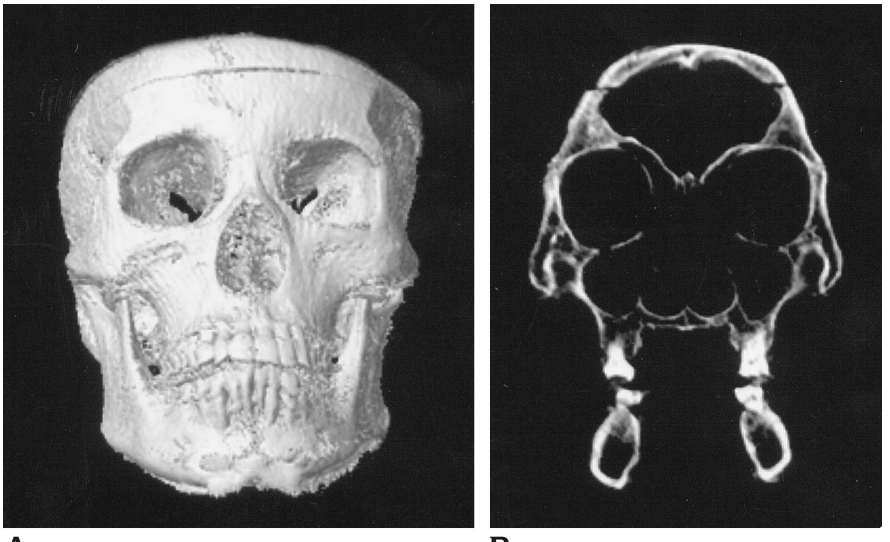

Fig 3. *A*, Anteroposterior view of the reconstructed 3-D volume of the human skull, shown in surface rendering. Some ripple on the surface is noted, which is due to the low number of projections used in the reconstruction.

B, A multiplanar reformatted section through the 3-D volume shown in texture map. Note the faithful reconstruction of fine bony detail.

Discussion

One of the main concerns when this system was originally under design was the total time required for injection of contrast material. Although a long injection time would necessitate a substantial volume of contrast agent, the total amount could be reduced by using contrast diluted to 50% or 25% of the original concentration (typically, 300 mg/mL of iodine). Even for a 6-second injection of full-strength contrast agent, the 18 mL required for a single 3-D reconstruction represents less than 20% of the average required for a standard angiographic (ie, noninterventional) procedure (13). Noninterventional procedures sometimes require as much as 200 mL of contrast material, and interventional procedures would generally be at the high end of the standard range. Of more concern was the replacement of blood by the contrast agent, with a potential for injury to the brain from oxygen debt accompanying a very long injection time. The modifications made to our high-speed unit reduced the total time required for data acquisition, thus shortening the required injection time to less than 5 seconds.

A second concern was the additional radiation dose to the patient that would be required for a single 3-D reconstruction of the intracranial vessels. From measurements made on an anthropomorphic phantom, we estimated that a tube current of 500 mA and an exposure time of 15 milliseconds per frame (100 frames total) would be required to produce adequate signal-to-noise ratio in a 3-D volume of human cerebral vessels. For our system, this corresponds to an entrance exposure of approximately 30 mGy, which is well below the limit for deterministic effects, such as temporary epilation (3 Gy) and erythema (6 Gy) (14–16). In addition, since the images are acquired during tube rotation, the entrance exposure is distributed over a large skin area, further reducing the deterministic effects of the imaging protocol (17).

In patients, conversion of the estimated entrance exposure to effective dose yielded a value of 0.1 mSv. This value corresponds to only 6% of the average total effective dose reported for patients undergoing treatment of an aneurysm with Guglielmi detachable coils (18). In fact, use of this computed rotational angiographic image technique may lead to an overall reduction in dose for the procedure, since the ability to visualize the 3-D volume from arbitrary angles (thereby obtaining an unobstructed view of the aneurysm's mouth) may reduce the number of digital subtraction angiographic (DSA) acquisitions required.

Several groups have combined the real-time imaging capabilities of XRII-based fluoroscopy with the advantages of 3-D CT by mounting an XRII on a CT gantry (19–21). This configuration avoids the problems of C-arm instabilities that we have addressed; however, the range of view angles available during fluoroscopy is limited by the CT gantry. In addition, this new equipment would be prohibitively expensive, because of the specialized gantry, and would not serve as an adequate replacement for conventional CT

in other, nonangiographic applications, owing to reduced precision (ie, increased noise reduces the ability to differentiate between different soft tissues).

An alternative method for producing 3-D reconstructions using a C-arm mounted XRII similar to ours has been proposed by other investigators (A. Sen, H. Hsiung, B. A. Schueler, M. S. Patel, R. E. Latchaw, X. Hu, "Three-dimensional Reconstruction of Vasculature with Limited Angiographic Projections" (abstract), *Radiology* 1995;197[P]:328). Their technique is based on the use of an algebraic algorithm to reconstruct the vasculature from a limited number of DSA projections. As with all DSA techniques, a doubling of the total time for image acquisition occurs, because two images at each angle are required, one for the mask and one during injection of contrast material. Since reconstruction is being performed from a limited number of views, the total radiation dose is not doubled as compared with our approach. Limited-view reconstruction algorithms perform best with subtracted projection views, making this approach very sensitive to image alignment errors and to patient motion between mask and contrast images. Reconstruction from subtracted images does have the advantage of removing the bone structures before reconstruction, circumventing the need for postreconstruction segmentation of the images; however, given the high contrast of the vessels in the 3-D images produced by using selective arterial injection, segmentation of bone without affecting the vasculature is relatively easy. Even in helical CT images, in which the injection is intravenous and vascular contrast is lower, removal of the bone has been done successfully (22). In addition, selective arterial injection generates a vascular signal well above the signal from the surrounding bone (on the order of 8000 HU in vessels compared with 2200 HU in bone), making our technique ideal for MIP rendering.

Comparison with conventional CT examinations indicates that our new imaging technique has several advantages. The most important is the ability to produce the 3-D images during the interventional procedure. A second is the possibility of acquiring all data necessary for reconstruction during a single breath-hold, which reduces the possibility of motion artifacts. In addition, since the contrast injection is selective, less contrast agent is required and the vessel contrast is increased. Because projection data are acquired using a 2-D detector, a volume covering more of the intracranial vasculature can be reconstructed from a single set of projection images, with an isotropic voxel size over the entire volume of interest, which is smaller than that attainable with any other currently available 3-D imaging technique. Although the pixel size is larger than that achieved with DSA, we consider the provision of 3-D images an augmentation to rather than a replacement for current 2-D imaging techniques. Additionally, for these preliminary investigations, we used the coarsest digitization mode of the XRII. In the future, we plan to generate reconstructions with pixels of approximately 0.25-mm isotropic cubes by using the high-resolution digitization mode. Finally, the modifications required to increase the velocity of rotation of the high-speed angiographic unit do not restrict the normal operation of the C-arm, thus preserving the usual choice of viewing angles during DSA cine imaging and real-time fluoroscopy.

In conclusion, we have developed true 3-D computed rotational angiography using an XRII system. The acquisition and reconstruction of data for this technique are feasible during neuroendovascular therapeutic procedures. Computed rotational angiography has the potential to enhance the understanding of geometric 3-D relationships between aneurysmal mouths and adjacent branches.

Acknowledgments

We are grateful to M. Westmore, J. Joire, H. Nikolov, A. B. Hashemi, N. Navab, K. Wiesent, and P. Durlak for helpful discussion leading to this work. B. Becker was instrumental in generating the reconstructions using the Feldkamp technique. L. Denning (animal health technologist), B. Lehrbass (registered X-ray technologist), and D. Rosso (clinical fellow, interventional neuroradiology) provided invaluable assistance with the in vivo experiments. The human skull was provided by the Phantom Labs, Salem, NY. The conventional angiographic unit was a Siemens Neurostar system; the high-speed angiographic unit was a Siemens Multistar unit modified by Siemens AG, Erlangen, Germany.

References

1. Aoki S, Sasaki T, Machida T, Ohkubo T, Minami M, Sasaki Y. Cerebral aneurysms: detection and delineation using 3-D CT. *AJNR Am J Neuroradiol* 1992;13:1115–1120
2. Dorsch N, Young N, Kingston RJ, Compton JS. Early experience

with spiral CT in the diagnosis of intracranial aneurysms. *Neurosurgery* 1995;36:230–238
3. Tsuruda JS, Sevick RJ, Halbach VV. Three-dimensional time-of-flight MR angiography in the evaluation of intracranial aneurysms treated by endovascular balloon occlusion. *AJNR Am J Neuroradiol* 1992;13:1129–1136
4. Tsuruda J, Saloner D, Norman D. Artifacts associated with MR neuroangiography. *AJNR Am J Neuroradiol* 1992;13:1411–1422
5. Kochli VD, McKinnon GC, Hofmann E, Von Schulthess GK. Vascular interventions guided by ultrafast MR imaging: evaluation of different materials. *Magn Reson Med* 1994;31:309–314
6. Tu RK, Cohen WA, Maravilla KR, et al. Digital subtraction rotational angiography for aneurysms of the intracranial anterior circulation: injection method and optimization. *AJNR Am J Neuroradiol* 1996;17:1127–1136
7. Parker DL. Optimal short scan convolution for fanbeam CT. *Med Phys* 1982;9:254–257
8. Feldkamp LA, David LC, Kress JW. Practical cone-beam algorithm. *J Opt Soc Am* 1984;1:612–619
9. Fahrig R, Holdsworth DW, Fox AJ. Characterization of a C-arm mounted XRII for 3D image reconstruction during interventional neuroradiology. *Proc SPIE* 1996;2708:351–360
10. Frayne R, Gowman LM, Rickey DW, et al. A geometrically accurate vascular phantom for comparative studies of x-ray, ultrasound, and magnetic resonance vascular imaging: construction and geometrical verification. *Med Phys* 1993;20:415–425
11. Smith RF, Rutt BK, Fox AJ, Rankin RN, Holdsworth DW. Geometric characterization of stenosed human carotid arteries. *Acad Radiol* 1996;3:898–911
12. Fox AJ. How to measure carotid stenosis. *Radiology* 1993;186:316–318
13. Dion JE, Gates PC, Fox AJ, Barnett HJM, Blom RJ. Clinical events following neuroangiography: a prospective study. *Stroke* 1987;18:997–1004
14. International Commission of Radiation Protection. *Nonstochastic Effect of Ionizing Radiation. ICRP Publication #41.* New York, NY: Pergamon Press, 1984
15. Huda W, Peters KR. Radiation-induced temporary epilation after a neuroradiologically guided embolization procedure. *Radiology* 1994;193:642–644
16. Wagner LK, Eifel PJ, Geise RA. Potential biological effects following high X-ray dose interventional procedures. *J Vasc Intervent Radiol* 1994;5:71–84
17. Norbash AM, Busick D, Marks MP. Techniques for reducing interventional neuroradiologic skin dose: tube position rotation and supplemental beam filtration. *AJNR Am J Neuroradiol* 1996;17:41–49
18. Bergeron P, Carrier R, Roy D, Blais N, Raymond J. Radiation doses to patients in neurointerventional procedures. *AJNR Am J Neuroradiol* 1994;15:1809–1812
19. Ning R, Kruger RA. Computer simulation of image intensifier-based computed tomography detector: vascular application. *Med Phys* 1988;15:188–192
20. Ning R, Wang X, Shen J, Conover KL. Image intensifier-based computed tomography volume scanner for angiography. *Acad Radiol* 1996;3:344–350
21. Saint-Felix DM, Trousset Y, Picard C, Ponchut C, Romeas R, Rougee A. In vivo evaluation of a new system for 3-D computerized angiography. *Phys Med Biol* 1994;39:583–595
22. Alberico RA, Ozsvath R, Casey S, Patel M. Helical CT angiography for the detection of intracranial aneurysms. *AJNR Am J Neuroradiol* 1996;17:1002